BEST AVAILABLE IMAGES

Defective images within this document are accurate representations of the original documents submitted by the applicant.

Defects in the images may include (but are not limited to):

- BLACK BORDERS
- TEXT CUT OFF AT TOP, BOTTOM OR SIDES
- FADED TEXT
- ILLEGIBLE TEXT
- SKEWED/SLANTED IMAGES
- COLORED PHOTOS
- BLACK OR VERY BLACK AND WHITE DARK PHOTOS
- GRAY SCALE DOCUMENTS

IMAGES ARE BEST AVAILABLE COPY.

As rescanning documents *will not* correct images, please do not report the images to the Image Problem Mailbox.

Multilayer antireflection coatings for the visible and near-infrared regions

H. Ganesha Shanbhogue, C. L. Nagendra, M. N. Annapurna, S. Ajith Kumar, and G. K. M. Thutupalli

With a high-refractive-index mixed-oxide dielectric material of $ZrTiO_4$ and ZrO_2 [Substance H2 (Sub2) from E. Merck, Darmstadt, Germany], in combination with magnesium flouride (MgF_2), design optimization and experimental production of low-loss antireflection (AR) coatings are carried out. Design-optimization studies that make use of these materials as constituents of a seven-layer coating system demonstrate that when the useful bandwidth of an AR coating is extended to cover a wider spectral range, the designs are in general found to have increased integrated reflection loss, higher ripple, and increased spectral instability. The experimental studies on Sub2 material show that the films have excellent optical performance over a wider process window, the advantage of which is demonstrated in the production of different AR coatings on a variety of glasses with refractive indices that range from 1.45 to 1.784 and different mechanical, thermal, and chemical properties. The manufacturing process of AR coatings shows a consistency better than 99% with respect to optical properties and durability. © 1997 Optical Society of America

1. Introduction

Visible and near-infrared antireflection (AR) coatings are indispensable to modern optical and electro-optical systems. The present trend in all these systems is to have improved optical performance over a wider spectral range, which makes it necessary to have efficient AR coatings with respect to residual reflection loss, transmission efficiency, spectral coverage that ranges from the visible to the near-infrared region, angle-of-incidence stability,[1–3] and durability against adverse terrestrial and space conditions.[2] Apart from these, the manufacturing process should have a high degree of consistency to enable easy reproducibility with consistent performance. As a result, AR coating development and applications call for a multidisciplinary approach, from design optimization to production techniques.

Visible and near-infrared AR coatings are studied from various view points,[3–10] which can be grouped under the following: (1) exclusive studies on the design optimization of AR coatings[3–7] and (2) application of different processing and monitoring techniques such as optical monitoring and high-energy ion-beam deposition and electron-beam evaporation.[8–11]

The former category of investigations has generated a wide range of efficient designs, generally confined to specific substrates that have refractive indices of 1.45 and 1.52. However, many of the designs fall short of realization in practice either because of the nonavailability of compatible stable/durable materials and the adaptability for generally available deposition techniques or because of complicated layer structures. These limitations restrict the whole range of efficient designs. The latter category of investigations has been successful in the application of different preparation and monitoring techniques that allow the production of efficient AR coatings. In spite of these extensive investigations, there are problems that have not been addressed and systematically studied. In particular, they are:

(1) AR coatings are required to be deposited on a variety of optical glasses that are known to have different refractive indices ranging from 1.45 to 1.8 and different chemical compositions, mechanical hardnesses and environmental stabilities.[12–14]

(2) Coatings that have different spectral efficiencies, in terms of residual reflection loss, transmission efficiency, and angle of incidence stability, are used for different situations.[2]

The authors are with the Laboratory for Electro-Optics Systems, Indian Space Research Organisation Satellite Center, A3-6, Peenya Industrial Estate, Bangalore 560 058, India.

Received 24 September 1996; revised manuscript received 4 February 1997.
0003-6935/97/256339-13$10.00/0

In addition, it may arise that a particular design and an experimental process, including materials and method of deposition, may not hold good for all variety of glasses because of diverse optical, chemical, and mechanical properties. The present investigation aims at studying systematically the design and development of visible and near-infrared AR coatings, focusing attention on the following specific problems: (1) Comprehensive design solutions for all varieties of AR coatings on different types of optical glasses, including a discussion of the impact on experimental production; and (2) Preparation/characterization of AR coatings on different types of known optical glasses, in which the scope of the materials and the method of deposition to produce efficient coatings are examined specifically.

Starting from a critical review of optical materials applicable for visible and near-infrared AR coatings, we present first the investigations of the preparation and characterization of optical thin films, namely Substance H2 (Sub2) from E. Merck, Darmstadt, Germany, and magnesium flouride (MgF_2), followed by design optimization of low-loss AR coatings. In design-optimization studies the interrelation among the various optical properties of optimized designs are specifically examined and presented. The production of AR coatings on different optical glasses and the AR coating's optical properties and durability are subsequently discussed. The consistencies in optical properties and durability of AR coatings are also highlighted.

2. Optical Material Combinations

In design and development of low-loss AR coatings, we need not emphasize the importance of the MgF_2 material that can be paired with other medium- and high-index materials such as silica (SiO_2), alumina (Al_2O_3), and oxides of tantalum, titanium zirconium, and niobium. Even though many efficient designs have been generated with these materials in a variety of ways,[3–7,15–17] a paired combination of MgF_2 and a high-index material is the preferred one. The high-index material is generally selected from oxides of titanium, tantalum, zirconium, and niobium to make use of the inherent advantages of a high-index ratio to produce efficient AR coatings.[3–6,16,17]

However, our critical review of the literature shows that each of these high-index oxides has a problem that affects the optical properties and the durability of the AR coatings. TiO_2 is prone to structural transformation, and the multilayer coatings that consist of TiO_2 have shown failures such as tensile fracture and delamination.[18] Tantalum pentoxide (Ta_2O_5) is susceptible to developing coating defects such as nodules[19] when it is deposited under the higher oxygen partial pressure and substrate temperatures (250–300 °C) that are invariably used to produce transparent coatings.[11,20] Zirconium oxide has a deficiency in that the optical layers are generally inhomogeneous, affecting the optical performance of the AR coatings.[21]

We believe that any of these problems, either alone or in combination, can play an adverse role in the development and production of multilayer AR coatings. Particularly in situations of large-volume production, the use of these oxides may affect the production efficiency because of the limited process window for efficient coatings. Even though niobium pentoxide (Nb_2O_5) has a refractive index higher than any other oxide material, there are reports of the application of this material in AR coating development with only reactive RF sputtering.[14,16] All these problems suggest the application of new materials for the development and production of multilayer AR coatings.

There are reports of investigations on homogeneous mixed-oxide dielectric thin films consisting of $ZrTiO_4$ and ZrO_2 (Sub1[21]) and composite optical coatings such as Ta_2O_5+SiO_2 (E. Merck, Germany), TiO_2+Ta_2O_5,[23] and SiO_2+TiO_2.[24,25] While the composite oxide coatings were prepared by codeposition techniques, the former is from a homogeneous mixed-oxide dielectric optical material of the same composition.[21] In composite optical coatings, the optical properties and the thickness of the coatings are highly sensitive to relative geometric positions of the individual source materials and the substrate, and the mixing ratios should be controlled within the desired limits to achieve homogeneous optical properties.[24] These two factors have adverse implications in the application of composite coatings for the development and the production of AR coatings. However, homogeneous mixed-oxide material, Sub1, can be used for the preparation of homogeneous optical coatings with an even simpler technique, electron-beam evaporation.[21] Therefore one of the objectives of our investigation is to explore the range of a material that belongs to this family for AR coating development and production.

3. Optical Material Preparation and Characterization

A. Refractive Index of Sub2 Thin Films

Sub2 optical coating material supplied by E. Merck is deposited on optically polished and cleaned quartz substrates by electron-beam evaporation. Prior to deposition the chamber is pumped to a base pressure of 10^{-5} mbar or better, and high-purity dry oxygen is allowed into the chamber in order to obtain a pressure of 10^{-4} mbar. Single-layer Sub2 films are deposited at an evaporation rate of 0.05–0.1 nm/s at a specific substrate temperature in the range from ambient to 250 °C. The substrate temperature is monitored to within an accuracy of ±2 °C. The deposited coating thicknesses are in the range 150–200 nm.

The optical properties of the films, namely reflectance R and transmittance T, are characterized with the Hitachi double-beam spectrophotometer, Model U-3400, over the wavelength range 400–2000 nm. The instrument is calibrated, *a priori*, to the reflectance and transmittance measurements. For the reflectance measurement, a 5° specular reflectance accessory is used. From the measured R and T data, refractive index n and absorption index k are evalu-

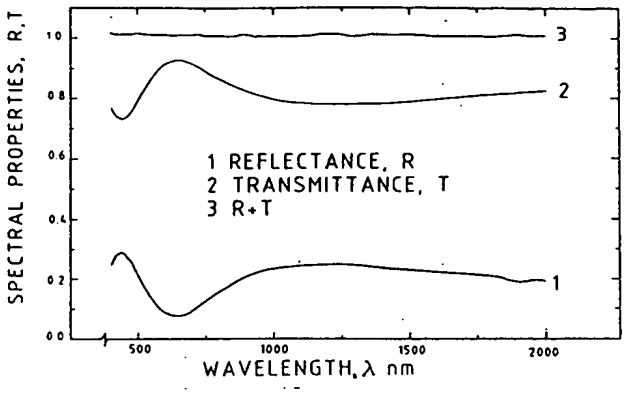

Fig. 1. Spectral properties for Sub2 thin films deposited at 200 °C.

ated by directly solving the R and T equations with the numerical iteration technique.[26] This results in the evaluation of n and k over the desired wavelength range for a preset value of film thickness, which may be either underestimated or overestimated.[27] However, by adapting the continuous dispersion curve criteria,[28] we determine the exact film thickness to an accuracy of 0.5 nm, which ultimately results in the determination of n and k values to within the accuracies of 0.005 and 0.002, respectively. These uncertainties are mainly caused by errors in the measurements of R and T.

In Fig. 1, the measured R and T values and the sum of the R and T values are presented for a film deposited at 200 °C. Note that the sum of the R and T values is equal to 1.0 ± 0.01 over the considered spectral range, indicating that the film is transparent. The refractive index and the associated unwanted solutions, derived from the optical constants evaluation, are shown in Fig. 2. Because the film is transparent, the derived absorption index values are not explicitly shown. They are, however, within 0.001. The film has a refractive index in the range of 2.1–1.95 over the spectral region 400–2000 nm.

The present values for Sub2 are close to those reported for Sub1,[21] which is the first version of homogeneous mixed-oxide dielectric material, consisting of $ZrTiO_4$ and ZrO_2 in a definite proportion. Even though the refractive-index values of Sub2 are close to those of Sub1, there are differences between the two, which are observed in the present investigation. Sub2 material melts like Ta_2O_5, prior to evaporation, while melting was hardly observed in Sub1. Also, smooth evaporation, devoid of spattering, was consistently observed in Sub2, contrary to the intermittent occurrence of spattering in Sub1. While the evaporation rate of Sub2 could be controlled easily within the range 0.1–0.2 nm/s, Sub1 exhibited considerable fluctuations in deposition rate.

It follows from examination of the dispersion curve and the associated multiple solutions in Fig. 2 that there are no abrupt breaks in the dispersion curve, which is a direct indication of the film being optically homogeneous[29] in contrast with the inhomogeneous nature of ZrO_2 films.[21] The substrate temperature dependence of the refractive index is presented in Fig. 3, where the refractive indices of the films, deposited at different substrate temperatures, are presented. It may be important to add that in these categories of films, which were prepared either at room temperature or at elevated temperatures, the sum of R and T never deviated from 1.0 ± 0.01, which is an advantageous feature of the Sub2 material not observed in other high-index optical materials such as oxides of Ti, Ta, and Zr. The earlier investigators observed, particularly in the case of Ta_2O_5,[11,20] that the films deposited at elevated temperatures ranging from 250 to 400 °C and at evaporation rates <0.25 nm/s are nonabsorbing and homogeneous, and at lower temperatures the films show signs of absorption and positive inhomogeneity. In light of this, the Sub2 material is more advantageous and has scope to produce transparent coatings at lower substrate temperatures, the feature of which is exploited in the present investigation.

From Fig. 3, one can see that while room-temperature films have the lowest refractive-index values, the films deposited at elevated temperatures have higher refractive-index values. Even though the room-temperature films are transparent, the

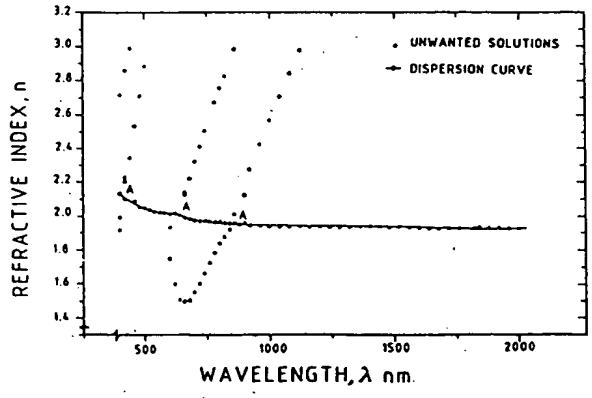

Fig. 2. Dispersion curve and associated multiple solutions for Sub2 thin films.

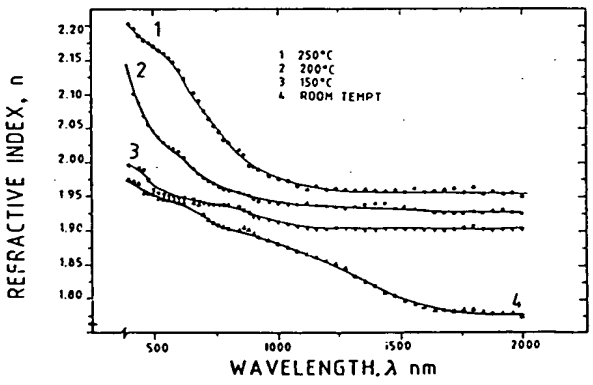

Fig. 3. Refractive index of Sub2 thin films deposited at different substrate temperatures.

Table 1. Dispersion Constants for Sub2 Films

Temperature (°C)	A	B (nm)^2 × 10^{-4}	C (nm)^4 × 10^{-9}
Ambient	1.82675	16.551	−20.367
150	1.89915	1.3320	0.33018
200	1.92211	1.3995	3.11842
250	1.94227	3.0956	1.6889

refractive-index values are as low as 1.8 in the near-infrared region. Also, the n values for films deposited even at elevated temperatures (200–250 °C) are lower than those for Ta_2O_5 and Nb_2O_5.[11,17,20] From the refractive-index data, dispersion constants are derived with a polynomial equation of the type $n = A + B/\lambda^2 + C/\lambda^4$, where A, B, and C are the Cauchy's dispersion constants and λ is the wavelength in nanometers. The dispersion constants are presented in Table 1. From the magnitude of the dispersion constants, it can be inferred that the films deposited at intermediate temperatures, 150–200 °C, are less dispersive.

B. Refractive Index of MgF_2 Thin Films

In the present investigation of multilayer AR coating development and production, we chose MgF_2 material as the low-index optical material. Even though the optical properties of MgF_2 thin films have been investigated extensively,[30–32] we reinvestigated to obtain *a priori* knowledge of the optical properties of the MgF_2 coatings prepared in our laboratory under specific deposition conditions intended to be used in the AR coating development and production. In view of the excellent optical properties of Sub2 coatings achieved at 200 °C, we propose that this substrate temperature also be used for the deposition of MgF_2 coatings.

Single-layer coatings of MgF_2 are deposited at 200 °C on plane-parallel glass substrates. During evaporation the deposition rate and the chamber pressure are maintained at 0.3–0.5 nm/s and 2×10^{-5} mbar, respectively. Optical transmittance of the deposited coatings is characterized in the manner described above. For evaluation of the refractive index of the coatings from the measured transmittance, only the peak transmittance T_{peak} at a particular wavelength λ_{peak} is considered. In fact λ_{peak} corresponds to the wavelength at which the reflectance of the coating is minimum. At this wavelength T_{peak} is a function of substrate refractive index n_s and film refractive index n_f and is independent of coating thickness. The exact form of the equation is given by[33]

$$T_{peak} = \frac{4.0\, n_f^2 n_s}{(n_f^2 + n_s^2)(n_f^2 + 1)}. \quad (1)$$

Equation (1) can be rewritten as

$$n_f^4 + A n_f^2 + n_s^2 = 0, \quad (2)$$

where $A = n_s^2 + 1 + (4n_s/T_{peak})$. Equation (2) can explicitly solve for n_f in terms of n_s and T_{peak}:

$$n_f = \left[\left(-A \pm \left\{\left[(n_s + 1.0)^2 - \left(\frac{4n_s}{T_{peak}}\right)\right] \times \left[(n_s - 1.0)^2 - \left(\frac{4n_s}{T_{peak}}\right)\right]\right\}^{1/2}\right)/2\right]^{1/2} \quad (3)$$

For a measured value of T_{peak}, one of the solutions corresponds to the refractive index of the film at the wavelength that corresponds to λ_{peak}. We adapted the above simple evaluation procedure for MgF_2 thin films rather than the more generalized procedure described in Subsection 3.A because our extensive studies of refractive-index evaluation of low-index coatings deposited on high-index substrate [such as ThF_4/Ge, CdSe/Ge, and CdTe/Ge (Ref. 26)] show that because of too many missing solutions at the regions corresponding to the intersection of the actual dispersion curve and the unwanted solutions (denoted by A in Fig. 2), continuous dispersion curve criteria cannot be applied precisely as in the case of high-index Sub2 films. Hence the refractive index of the coating cannot be determined accurately. The present evaluation procedure is devoid of these complications. Therefore, following this procedure, we evaluated refractive indices of the MgF_2 coatings deposited on different glass substrates and the results are presented in Table 2.

From Table 2 results it follows that the refractive index of the MgF_2 thin films is close to 1.35 ± 0.01 over the wavelength range 500–900 nm, which is observed irrespective of the substrate on which the films are deposited. Note that the present values are lower compared with the extensively reported values of 1.38–1.37 in the literature for a similar category of films.[30–32] To investigate the reasons for this discrepancy, we evaluated the probable deviations Δn_f owing to uncertainties in the T_{peak} measurement (see Table 2). Values of Δn_f are within +0.013 and −0.014 and +0.029 and −0.034 corresponding to ±0.2% and ±0.5% measurement errors, respectively, for films deposited on low-index quartz substrates. These values tend to be higher for films deposited on higher-index substrates. Because a small error in the transmittance measurement can cause larger deviations in n_f, the observed difference between our results and the reported values can be attributed to measurement uncertainties. Because our results are close to 1.35 ± 0.01, the refractive index value of the MgF_2 layers is set to 1.35 in the design-optimization exercises and in the subsequent calculations related to theoretical and experimental comparison.

4. Design Optimization

The aim of the design-optimization exercise is to generate low-loss AR coating designs, which are useful in visible and near-infrared regions, on glass substrates that have refractive indices in the range 1.45–1.784. We are limited here in that the ultimate designs are required to be based on a single

Table 2. Refractive Index of MgF_2 Coatings on Different Glasses at Different Wavelengths[a]

Glass	Refractive Index N_s	λ_{peak} (nm)	T_{peak} (%)	n_{MgF_2}	Δn for $\Delta T = \pm 0.0005$	Δn for $\Delta T = \pm 0.002$
Quartz	1.450	445	95.05	1.375	−0.034	−0.013
					+0.029	+0.012
	1.450	470	95.37	1.355	−0.030	−0.012
					+0.026	+0.011
	1.450	496	95.21	1.363	−0.033	−0.012
					+0.028	+0.011
	1.450	530	95.22	1.362	−0.030	−0.012
					+0.026	+0.011
	1.450	610	95.27	1.359	−0.033	−0.012
					+0.029	+0.011
	1.450	730	95.32	1.356	−0.034	−0.013
					+0.029	+0.012
	1.450	740	95.39	1.357	−0.034	−0.013
					+0.029	+0.012
	1.450	920	95.48	1.346	−0.034	−0.014
					+0.029	+0.013
UBK7	1.550	420	94.29	1.387	−0.040	−0.014
					+0.040	+0.014
	1.520	690	94.93	1.363	−0.036	−0.025
					−0.051	+0.013
UBK7	1.520	740	95.00	1.349	−0.036	−0.016
					+0.051	+0.017
	1.520	1230	95.08	1.342	−0.038	−0.014
					+0.051	+0.014
SK16	1.618	502	94.08	1.361	—	−0.036
					+0.056	+0.015
	1.618	550	94.11	1.350	—	−0.031
					+0.046	+0.023
	1.618	790	94.05	1.358	—	−0.028
					+0.051	+0.021
SK16	1.618	820	94.13	1.348	—	−0.033
					+0.055	+0.022
SF2	1.688	420	92.79	1.385	—	−0.029
					+0.050	+0.023
	1.640	700	93.85	1.354	—	−0.029
					+0.50	+0.023
LAFN21	1.784	650	92.05	1.356	—	—
					+0.089	+0.049

[a]Substrate temperature is 200 °C.

multilayer configuration that essentially consists of MgF_2 and Sub2 coating materials in alternate sequence.

Generally in the visible and near-infrared regions two types of AR coatings are of interest, namely, (1) wideband (WB) AR coatings that cover both the visible and the near-infrared regions and (2) limited-band (LB) AR coatings that operate at discrete spectral bands such as 620–680 nm and 770–860 nm. While the WB AR coatings are used in many advanced space-borne electro-optical systems such as star sensor optics and imaging spectrometers[34,35] and in industrial optical systems such as infrared and visible photographic cameras,[3] the LB AR coatings are used in high-resolution imaging cameras in discrete spectral bands.[13] The WB AR coatings are required to have wider spectral coverage and maintain a low average-reflection loss, $R_{av} < 0.5\%$, and a high average transmission, $T_{av} > 98\%$; whereas LB AR coatings should have a very low reflection loss, $R_{av} < 0.2\%$, and a higher transmission $T_{av} > 99\%$. We intend to demonstrate these dual requirements using the same multilayer configuration.

To carry out the design optimization, we considered a seven-layer system consisting of an alternate sequence of MgF_2 and Sub2, with MgF_2 being the outermost layers adjacent to the medium and the substrate. Although more complex multilayer configurations may yield efficient designs in terms of residual reflection loss and spectral bandwidth,[3,16] we chose the seven-layer system because of its simplicity, easy adaptability for the manufacturing process, and shorter process turnaround time. The refractive index of MgF_2 is set to 1.35 as derived from the refractive-index evaluation of single-layer MgF_2 films, and n of Sub2 is derived from Cauchy's dispersion relation, the constants of which are set to those corresponding to 200 °C, given in Table 1. For design optimization, we used the software OPTOSOFT.

Table 3. Optimized Thickness Parameters for Multilayer Antireflection Coatings

Type of glass N_s	Type of Design	t_1 MgF_2 (nm)	t_2 Sub2 (nm)	t_3 MgF_2 (nm)	t_4 Sub2 (nm)	t_5 MgF_2 (nm)	t_6 Sub2 (nm)	t_7 MgF_2 (nm)
Fused	LB	144.0	166.0	29.1	21.0	14.0	11.0	29.0
Quartz	WB	120.4	137.8	15.4	12.8	15.4	12.8	225.4
1.450	EWB	125.4	167.8	45.4	12.8	10.4	12.8	65.4
UBK7	LB	149.0	181.0	24.0	26.0	24.0	11.0	14.0
1.520	WB	120.4	142.8	10.4	12.8	25.4	12.8	225.4
	EWB	120.4	162.8	45.4	17.8	255.4	12.8	40.4
SK16	LB	149.0	186.0	19.0	21.0	14.0	16.0	14.0
1.618	WB	115.4	137.8	25.4	17.8	245.4	12.8	25.4
	EWB	120.4	162.8	45.4	12.8	195.4	12.8	40.4
SF2/KZFSN5	LB	154.0	186.0	19.0	31.0	14.0	11.0	14.0
1.680	WB	120.4	157.8	15.4	12.8	15.4	12.8	10.4
	EWB	115.4	152.8	30.4	17.8	235.4	12.8	35.4
LAK10	LB	154.0	196.0	14.0	26.0	14.0	16.0	14.0
1.716	WB	120.4	157.8	10.4	17.8	10.4	12.8	10.4
	EWB	120.4	152.8	40.4	12.8	230.4	12.8	30.4
SF55	LB	154.0	191.0	14.0	31.0	14.0	16.0	14.0
1.754	WB	120.4	157.8	10.4	17.8	10.4	12.8	10.4
	EWB	115.4	142.8	25.4	17.8	235.4	17.8	30.4
LAFN21	LB	154.0	201.0	14.0	26.0	14.0	21.0	14.0
1.784	WB	115.4	162.8	15.4	22.8	10.4	12.8	10.4
	EWB	120.4	157.8	45.4	12.8	220.4	17.8	35.4

OPTOSOFT makes use of a quadratic merit function (MF) defined by

$$\mathrm{MF} = \left\{ \sum [(R_t - R_i) W_i]^k \right\}^{1/k}, \qquad (4)$$

where R_t is the target reflectance, R_i is the instantaneous reflectance, and W_i is the relative weight factor that is defined by either $W_i = R_t/R_i$ or $W_i = R_i/R_t$, depending on whether $R_t > R_i$ or $R_i > R_t$.[37] k is the MF index, which can be set to any one value such as 2, 4, 8, or 16. The summation is carried out over m wavelength points. This is set to 80 in the present analysis. Generally R_t equals 0.0001 in the spectral range of interest, in the design optimization of WB and extended wideband (EWB) designs; whereas it is assigned a zero value in LB designs and specific nonzero values in the shoulder region. R_i is evaluated with the well-known reflectance equation for multilayer thin-film systems.[38]

When we consider a typical quarter-wave ($\lambda_0/4$) stack (λ_0 equals 700 nm in WB and EWB designs and 800 nm in LB designs) as the starting design, the MF optimization is carried out with a unidirectional single-variable search technique, the coordination descent technique,[39,40] in which the MF is minimized with respect to a particular variable by successive comparison of the instantaneous value of the MF with the preceding value when all other variables are kept constant. This results in the minimization of the MF for a particular variable. The procedure is repeated for all the unknown variables, namely geometrical thicknesses, in a cyclic order. Repetition of the entire investigation over two or three cycles yields an optimized design.

Following this procedure, we generated three varieties of designs, namely LB, WB, and EWB, on different hypothetical substrate refractive indices that are equivalent to fused quartz (FQ) and to UBK7/BK7, SF2, KZFSN5, LAK10, SF55, and LAFN21 (brand names of glasses manufactured by Schott Glass Technologies, Mainz, Germany), in which identical input conditions are maintained for the design optimization of a particular design category. However, for generating WB and LB designs, k equals 2; EWB designs are obtained by considering k equal to 8. The results of design optimization, specifically optimized thickness parameters obtained for different designs on different substrate refractive indices, are presented in Table 3. Even though we obtain the thickness parameters by setting the refractive index of MgF_2 equal to 1.35, these parameters can also be used for the seven-layer system, with the refractive index of the MgF_2 coating equal to 1.38, the validity of which we show below.

Spectral reflectance of a few optimized designs on substrates with refractive indices equal to 1.618 and 1.754 are shown in Figs. 4(a) and 4(b), respectively. The results show that, starting from a seven-layer configuration, both WB and LB designs are obtained. Also, in LB designs, there is a gradual variation of reflectance, whereas in WB designs, a nonuniform reflectance variation associated with ripple, that is, reflectance maximum R_{max}, is observed. Similar reflectance characteristics are generated for all designs given in Table 3 from which salient spectral properties [namely spectral bandwidth ratio (SBWR) ($\lambda_U - \lambda_L$), where λ_U and λ_L are the upper and the lower wavelength limits within which $R \leq 1.0\%$, 0.5%, and 0.2%; integrated reflection loss (IRL) R^*; maximum reflectance R_{max}; and minimum reflectance R_{min}] are evaluated. For calculation of IRL R^*, which also

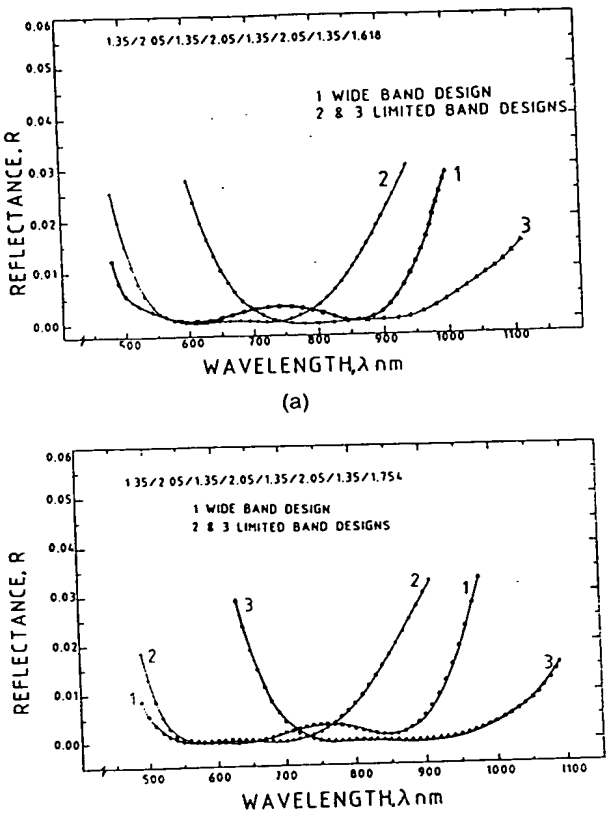

Fig. 4. (a) Reflectance characteristics of optimized designs on a hypothetical substrate; refractive index 1.618. (b) Reflectance characteristics of optimized designs on a hypothetical substrate; refractive index 1.754.

represents the average reflection loss R_{av} within a defined band, numerical integration of

$$R^* = \int_{\lambda_L}^{\lambda_L} R(\lambda)\mathrm{d}\lambda \Big/ \int_{\lambda_L}^{\lambda_U} \mathrm{d}\lambda \qquad (5)$$

is carried out over a defined bandwidth within which $R \leq 1.0\%$, 0.5%, and 0.2%.

The results of the optical properties of the designs, namely SBWR (λ_U/λ_L), IRL R^*, R_{max}, and R_{min}, are presented in Table 4, from which it follows that LB designs have the lowest spectral coverages, SBWR values range from 1.355 to 1.393 (overall seven designs on different substrates) for $R \leq 0.2\%$, the lowest IRL value ranges from 0.04 to 0.055% for $R \leq 0.2\%$, and the lowest R_{max} ranges from 0.003 to 0.02%, thereby satisfying the design goal characteristics of very low residual reflection loss. Even though the design value of the IRL is 2 orders of magnitude lower than the acceptable limit of 0.2% residual reflection loss for LB AR coatings, such design features are necessary for achieving the required performance in practice; we present the corresponding experimental results in Section 5. The EWB designs have very wide spectral coverage (SBWR ranges from 1.889 to 1.98 for $R \leq$ 1.0%), higher IRL (from 0.221 to 0.372%), and higher R_{max} (0.21 to 0.67%). The WB designs have values intermediate to LB and EWB designs. Even though WB and EWB designs have ripple higher than LB designs, in some cases exceeding the tolerable limit of 0.5% (EWB designs for FQ, UBK7, and LAK10), the corresponding IRL values are lower than the set limit of 0.5%. Because in the majority of applications of WB AR coatings the average optical properties within the useful band are more important than the properties at individual wavelengths, such designs can also find applications in practice.

The present design-optimization results are applicable to the multilayer system in which the refractive index of MgF_2 layers is equal to 1.35. However, most of the published values for MgF_2 thin films are close to 1.38.[30,32] In view of this, the application of the present optimized thickness parameters for multilayer systems with n_{MgF_2} equal to 1.38 is verified, for which the geometrical thickness of the MgF_2 layers is reevaluated with the relation $t_{1.38} = 1.35t_{1.35}/1.38$ ($t_{1.35}$ is the MgF_2 layer thickness from Table 3). Then the optical properties of the designs are evaluated and compared with the results given in Table 4 from which it is seen that in general there is a marginal increase in SBWR, IRL, and ripple R_{max}. For example, in EWB designs, the maximum increase in SBWR is 3% over the parent values, and the increase in IRL is within 0.05% (absolute change), whereas the increase in R_{max} is in the range 0.04–0.25% (absolute change). It follows that the present results can be applied also to a situation with n_{MgF_2} equal to 1.38, with only marginal changes in the spectral properties of the designs.

A close study of the results of SBWR and IRL presented in Table 4 shows that for a given design IRL, R^* is directly proportional to SBWR. The proportionality of variation is quasi-linear in the case of LB designs, as is evident from the results in Fig. 5. The degree of nonlinearity increases in WB and EWB designs. Correlation of SBWR values with ripple R_{max} indicates that the increase in useful bandwidth is invariably associated with higher-ripple R_{max}. This, however, is not an unfavorable feature as long as the average residual reflection loss R_{av}/IRL satisfies the design goal requirements, as explained in the previous paragraph. In fact, most WB and EWB designs fall into this category, which is evident from the corresponding results given in Table 4. The substrate refractive index does not have any substantial effect on the optical properties of the designs; this is a natural consequence of the optimized designs.

Spectral instability, or its reciprocal property spectral stability, of AR coating designs is a useful input for the production of AR coatings. It is expressed quantitatively in terms of spectral reflectance change ΔR, at one or more than one wavelength, for predetermined thickness and refractive index changes, either alone or in combination.[41] For the AR coating discussed here, which are useful over a spectral band, spectral instability is assessed by normalized spectral deviation (NSD) defined by

$$\Delta R = \left[\sum \frac{\Delta R_i}{(\lambda_U - \lambda_L)}\right]\delta\lambda, \qquad (6$$

Table 4. Summary of Optical Properties of Different Designs

Type of Glass N_S	Type of Design	SBWR (λ_U/λ_L) $R \le 1\%$	SBWR (λ_U/λ_L) $R \le 0.5\%$	SBWR (λ_U/λ_L) $R \le 0.2\%$	IRL R^* (%) $R \le 1\%$	IRL R^* (%) $R \le 0.5\%$	IRL R^* (%)$R \le 0.2\%$	R_{max} (%)	R_{min} (%)
Fused	LB	1.565	1.456	1.355	0.245	0.125	0.055	0.003	0.0008
Quartz	WB	1.730	1.618	1.438	0.220	0.119	0.062	0.140	0.004
1.450	EWB	1.960	1.830	1.713	0.301	0.251	0.232	0.670	0.08
UBK7	LB	1.624	1.500	1.382	0.229	0.113	0.044	0.01	0.0002
1.520	WB	1.820	1.745	1.667	0.222	0.153	0.132	0.32	0.03
	EWB	1.922	1.798	1.385	0.372	0.303	0.200	0.50	0.007
SK16	LB	1.634	1.489	1.380	0.263	0.107	0.045	0.005	0.0009
1.618	WB	1.820	1.733	1.651	0.252	0.151	0.121	0.19	0.02
	EWB	1.971	1.824	1.616	0.233	0.160	0.112	0.21	0.003
SF2/KZFSN5	LB	1.586	1.468	1.358	0.226	0.111	0.044	0.003	0.00
	WB	1.666	1.545	1.445	0.220	0.108	0.060	0.08	0.002
1.640	EWB	1.920	1.762	1.563	0.298	0.219	0.191	0.353	0.015
LAK10	LB	1.618	1.489	1.393	0.233	0.100	0.040	0.02	0.001
1.716	WB	1.626	1.501	1.404	0.196	0.115	0.052	0.061	0.014
	EWB	1.918	1.806	1.438	0.343	0.294	0.250	0.517	0.0002
SF55	LB	1.588	1.468	1.362	0.231	0.111	0.041	0.006	0.000
1.754	WB	1.66	1.505	1.408	0.175	0.107	0.049	0.04	0.002
	EWB	1.889	1.784	1.660	0.221	0.153	0.122	0.31	0.0005
LAFN21	LB	1.60	1.465	1.353	0.245	0.111	0.05	0.01	0.004
1.784	WB	1.70	1.481	1.366	0.230	0.177	0.118	0.10	0.06
	EWB	1.98	1.901	1.529	0.290	0.180	0.100	0.27	0.09

where ΔR_i is the spectral deviation at a particular wavelength λ_i, λ_U and λ_L are the wavelength limits within which R is <0.5%, and $\delta\lambda$ is the wavelength increment considered for summation. ΔR_i is evaluated by first determining the first-order reflectance derivatives with respect to the thickness and the refractive index of all layers from which absolute reflectance deviations are calculated from predetermined thickness and refractive index deviations. Summation of absolute deviations resulting from all layers yields ΔR_i at a particular wavelength.

In the present analysis, coating refractive-index deviations are set to 0.005 and thickness deviations are assigned a uniform value of 1.0 nm for layers whose thicknesses are >100 nm. For layers whose thicknesses are in the range 10–40 nm, the deviations are set to 0.5 nm. We chose these deviations by considering the tolerances that can be achieved in practice using quartz/optical thickness monitoring.[5] The results of NSD are presented in Fig. 6, where each point corresponds to the NSD obtained for a particular glass and for a particular design belonging to either the LB, the WB, or the EWB category. From the results it follows that LB designs have constant NSD values in the range 0.060–0.065%. In EWB and WB designs, NSD values are higher and vary over a wider range within which EWB designs have the highest NSD values and the widest variation. The range of variation is from 0.083 to 0.148% with respect to WB designs, whereas it is from 0.13 to 0.28% in the case of EWB designs. The higher NSD values associated with higher-ripple R_{max} in WB and EWB designs can be attributed to nonuniform reflectance variation, which can be obvious from[41]

$$\delta R/\delta\lambda = [\delta R/\delta(n_i, d_i)][\delta(n_i, d_i)/\delta\lambda].$$

$\delta R/\delta\lambda$ is the first-order reflectance derivative with respect to λ and $\delta R/\delta(n_i, d_i)$ is the first-order reflectance derivative with respect to either the thickness or the refractive index of the ith layer.

When the design has substantial ripple R_{max}, $\delta R/\delta\lambda$ is higher compared with a design with no ripple. From the preceding equation, it follows that $\delta R/\delta(n_i, d_i)$ is higher, resulting in higher NSD's for designs with higher R_{max}. The results of NSD's and the associated ripples R_{max} were fitted to a third-degree polynomial equation; see Fig. 6.

Regarding AR coating production, LB designs allow for better reproducibility in view of the fewest anticipated changes in spectral properties owing to inherent manufacturing errors in coating thicknesses and refractive indices. In WB and EWB designs, consider-

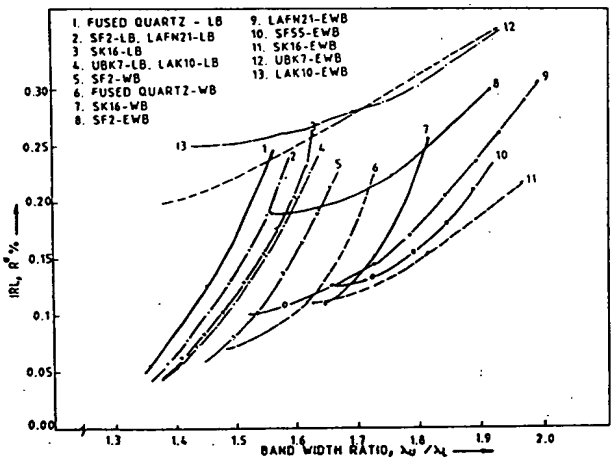

Fig. 5. Variation of IRL R^* with respect to SBWR for different AR coating designs.

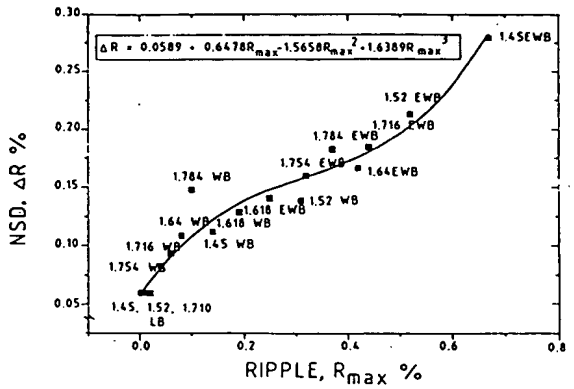

Fig. 6. NSD for AR coating designs with ripple R_{max}.

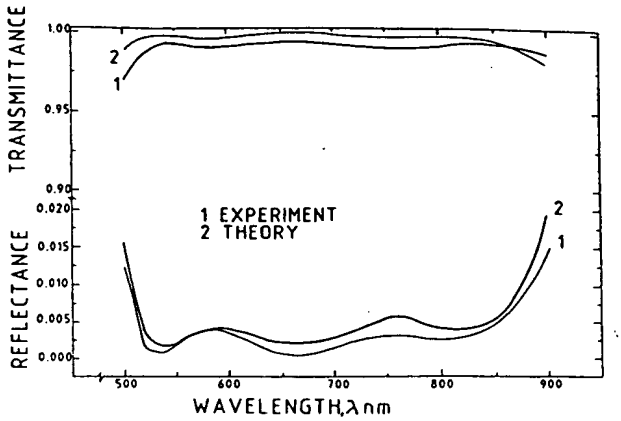

Fig. 7. Experimental results of a WB AR coating on SK16 glass and comparison with theory.

able scatter in optical properties can be expected as a result of theoretically observed higher NSD's.

5. Experimental Investigation

The purpose of the present experimental investigation is the study of the problems of development of WB and LB AR coatings on different optical glasses with different mechanical, thermal, and chemical properties and the characterization of the optical properties of the AR coatings, together with theoretical comparison. The problem is also focused on an investigation of the production efficiency of the coatings. The AR coatings are prepared in a Leybold Hereaus vacuum evaporation plant Model 560L by the electron-beam evaporation technique. The multilayers of MgF_2 and Sub2 are deposited at a 200 ± 5 °C substrate temperature on optically polished and cleaned glass substrates. The evaporation rates of MgF_2 and Sub2 are maintained at 0.3–0.5 nm/s and 0.05–0.1 nm/s, respectively. The thicknesses are monitored with a quartz crystal monitor, which is calibrated *a priori* to ensure deposition of the correct thicknesses as dictated by the design. The samples are generally recoated on the second surface of the substrates that are used for the study of the optical properties and the durability of the coatings.

The optical reflectance and transmittance of the coatings are studied with a UV-visible and near-infrared spectrophotometer, as explained above. Durability tests, namely high-temperature humidity, thermal shock/cycling, and hot–cold soak, are carried out in appropriate environmental chambers; and optical properties are verified before and after each test. Generally, five samples are used for the investigation, and an average of the measured property over the five samples is considered as the true measured value.

6. Results and Discussion

The optical properties of WB and LB AR coatings deposited on SK16 (n_s = 1.618) glass are shown in Figs. 7 and 8 along with the theoretical results from which it can be seen that theoretical and experimental results agree with each other within the limits of experimental error. Note that even though the LB AR coating design on a substrate equivalent to SK16 has reflection loss varying from 0.0009 to 0.005%, the observed value is in the range 0.1–0.2% (residual reflection loss per surface) over the desired spectral range 760–860 nm. Such a difference is mainly due to either the inherent error in reflectance measurement or in manufacturing, or both. Similar close correlation between theory and experiment is observed on AR coatings deposited on all other glasses except the KZ series.

The KZ series of glasses, manufactured by Schott, are generally soft glasses, which are more vulnerable to stain formation and have a lower glass transition temperature. However, these glasses are often chosen in advanced refractive multielement lens systems because of their compatibility with other medium-index glasses with respect to relative dispersion.[42] AR coating development on these glasses is not as routine as in other glasses and is in need of systematic study. In the present investigation, preparation and characterization of one such type of glass, KZFSN5, is studied in detail.

AR coatings are deposited at different substrate temperatures, and the spectral reflectance and transmittance of the coatings are characterized over the

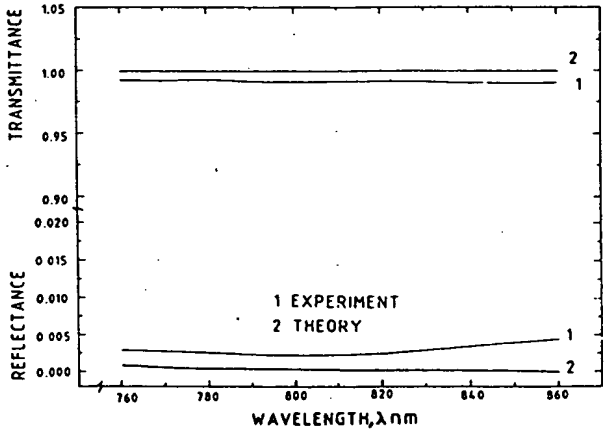

Fig. 8. Experimental results of a LB AR coating on SK16 glass and comparison with theory.

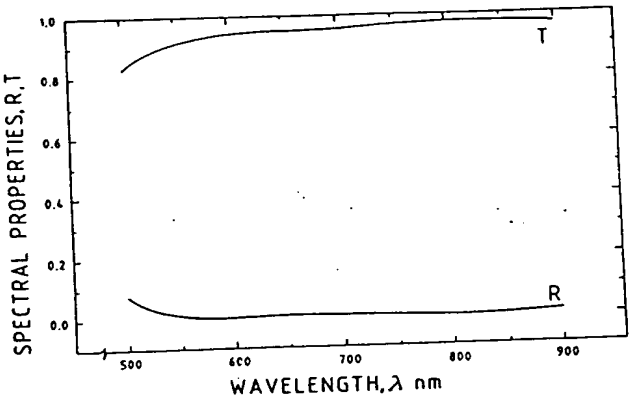

Fig. 9. Spectral reflectance and transmittance of a WB AR coating on KZFSN5 glass.

wavelength range 500–900 nm. The results of reflectance R and transmittance T for a WB AR coating deposited at 200 °C are shown in Fig. 9. The results show that, while the AR coating on a double-side-coated KZFSN5 plate is able to suppress the reflection loss of the substrate, from 11% to <1% in the wavelength range 550–900 nm, the transmittance is hardly better than 97% in the near-infrared and 95% in the visible region, which indicates an apparent absorption in the deposited AR coatings.

The absorption loss spectrum, calculated with $A = 1 - R - T$, is presented in Fig. 10, which shows that the absorption loss is considerably higher in the lower wavelength range. The substrate temperature dependence of A is also shown in Fig. 10, in which the absorption losses A that correspond to films deposited at different substrate temperatures are compared. It follows from these results that the loss is at a minimum at an intermediate substrate temperature (100 °C). This absorption loss might have been caused by the substrate because such absorption losses are not observed in coatings deposited on all other glasses.

To substantiate this, bare KZFSN5 samples are subjected to ion cleaning and heating cycles as are experienced in a coating-deposition cycle, and the absorption loss ($A = 1 - R - T$) spectra are analyzed. The corresponding results for 200 °C are shown in Fig. 11 along with those for samples subjected to glow discharge cleaning. It is obvious from the results that the heated substrate shows an absorption of ~2–3% in the visible spectrum, which is reduced to <0.5% in the near-infrared spectrum. This is responsible for the apparent absorption loss of the AR coatings in which two heating cycles result in a minimum absorption of 4–6%. The observation of absorption loss, in the range 0.5–1.0%, for samples subjected to glow discharge cleaning is attributed to substantial heating of the substrate during the ion-cleaning process. From this it is obvious that to ensure a minimum of absorption loss in AR coatings on the KZ series glasses, the coatings are required to be deposited at medium substrate temperatures, obviating glow discharge cleaning. This procedure is also required to be implemented strictly so that the glass transition temperature of these glasses is lower (T_g = 473 °C),[42] and the glasses should never exceed half of this temperature in order that the optical figure parameters of the components remain unaffected.

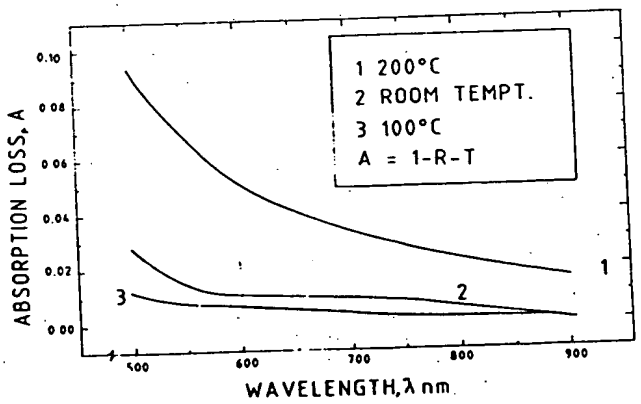

Fig. 10. Absorption loss characteristics of AR coatings deposited at different substrate temperatures.

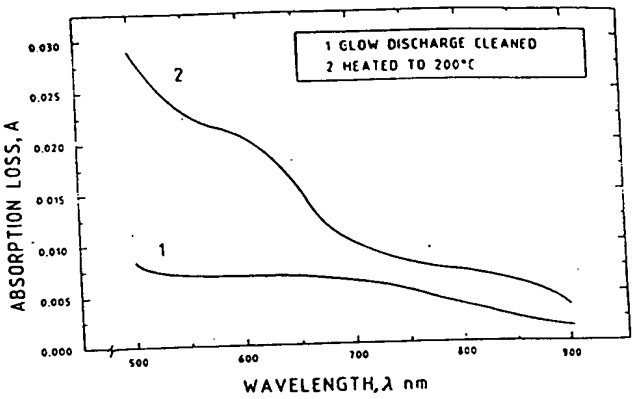

Fig. 11. Absorption loss spectrum of bare KZFSN5 plates.

It is possible to implement this condition and to achieve optically efficient AR coatings when Sub2 is used for the AR coating process because we can achieve efficient optical properties by adapting a medium substrate temperature in the range 100–120 °C as suggested by the present studies. These coatings, despite their lesser abrasion resistance, are found to withstand all other durability tests. Production of such low-absorption-loss AR coatings without affecting the optical components may not be possible to realize by the use of other high-index optical materials such as TiO_2 and Ta_2O_5 because these materials require substantially higher substrate temperatures to produce coatings with efficient optical properties.[11,20]

The WB and LB AR coatings are deposited on some important Schott glasses, namely FQ, UBK7, SK16, SF2, KZFSN5, LAK10, SF55, and LAFN21, with the design data given in Table 3 as the base. WB designs are favored over EWB designs because they fulfill our application requirements and show better reproducibility in practice because of lower NSD's.

Table 5. Optical Properties of WB AR Coatings: Theory and Experiment Compared[a]

Optical properties	Quartz	UBK7	SK16	SF2	KZFSN5	LAK10	SF55	LAFN21
$\lambda_U - \lambda_L$ (nm)								
T	380	420	400	340	340	340	350	380
E	380	420	415	360	390	360	340	420
λ_U/λ_L								
T	1.73	1.820	1.82	1.67	1.67	1.63	1.66	1.70
E	1.704	1.803	1.86	1.67	1.71	1.67	1.63	1.82
R_{min} (%)								
T	0.01	0.03	0.02	0.00	0.00	0.014	0.00	0.07
E	0.18	0.15	0.10	0.15	0.13	0.16	0.08	0.12
R_{max} (%)								
T	0.14	0.32	0.20	0.08	0.06	0.06	0.04	0.10
E	0.25	0.51	0.50	0.44	0.47	0.31	0.41	—
IRL/R_{av} (%)								
T	0.22	0.22	0.25	0.22	0.12	0.196	0.175	0.23
E	0.32	0.41	0.45	0.40	0.30	0.4	0.44	0.27
T_{av} (%)								
T	99.56	99.56	99.50	99.56	99.76	99.608	99.65	99.54
E	99.3	99.2	99.20	98.9	98.4	98.8	98.6	98.9
A	0.06	0.00	0.000	0.3	1.00	0.40	0.52	0.56

[a] R_{av}, average reflectance per surface within band; T_{av}, average transmittance within band; *T*, theory, *E*, experiment; $A = 1 - 2R_{av} - T_{av}$.

The salient results of the study of reflectance and transmittance of AR coatings are summarized in Table 5 for WB AR coatings and in Table 6 for LB AR coatings, along with the theoretical results. Table 5 shows that the theoretical and experimental results are in reasonable agreement with each other with respect to bandwidth and bandwidth ratio. However, experimental values are on the higher side in the case of R_{min}, R_{max}, and IRL/R_{av}. The maximum observed deviation in the case of R_{min} is 0.17% (for FQ glass) and 0.41% (for KZFSN5) in the case of R_{max}. The observed maximum deviation in IRL, R^*/R_{av}, from theory is 0.24% (for SF55 glass). These deviations are, however, within the limit of measurement error of 0.5%, which indicates good agreement between theory and experiment. The maximum observed deviation in T_{av} among low- and medium-index glasses such as FQ, UBK7, and SK16 is 0.36% whereas the deviations are in the range 0.66–1.36% for the rest of the glasses. However, an examination of the unaccounted losses ($1 - 2R_{av} - T_{av}$), where R_{av} is the average reflectance per surface and T_{av} is the

Table 6. Optical properties of LB AR Coatings: Comparison with Theory and Experiment Compared[a]

Optical properties	Fused Quartz	UBK7	SK16	SF2	LAK10	SF55
$\lambda_U - \lambda_L$ (nm)						
T	250	275	270	265	285	260
E	225	230	240	220	250	240
λ_U/λ_L						
T	1.355	1.382	1.380	1.358	1.393	1.356
E	1.321	1.330	1.340	1.310	1.351	1.330
R_{min} (%)						
T	0.0008	0.0002	0.0009	0.0000	0.001	0.000
E	0.17	0.110	0.100	0.100	0.140	0.100
R_{max} (%)						
T	0.003	0.010	0.005	0.003	0.02	0.006
E	0.220	0.320	0.440	—	0.26	—
IRL/R_{av} (%)						
T	0.055	0.044	0.045	0.044	0.04	0.041
E	0.200	0.200	0.170	0.130	0.21	0.150
T_{av} (%)						
T	99.89	99.912	99.91	99.912	99.92	99.918
E	99.540	99.40	99.4	99.40	99.20	99.20
A (%)	0.06	0.200	0.260	0.340	0.38	0.50

[a] R_{av}, average reflectance per surface within band; T_{av}, average transmittance within band; T, theory; E, experiment; $A = 1 - 2R_{av} - T_{av}$.

average transmittance over a given bandwidth, which are given in the last rows of Tables 5 and 6, shows that it is <0.06% for low- and medium-index glasses (FQ, UBK7, and SK16). The values are not beyond 0.6% in the rest of the glasses. The observed higher value (1.0%) of A in the case of KZFSN5 glass can be due to the residual absorption in the substrate induced during deposition of the coating, as we explained above.

From the summary of the optical properties of LB AR coatings presented in Table 6, it follows that all the LB AR coatings have an average reflection loss of <0.2% and a transmission efficiency of ≥99.4% in low- to medium-index glasses and 99.2% in high-index glasses, in contrast with the observed R_{av} in the range 0.27–0.45% and transmittance in the range 98.4–99.3% for WB AR coatings. This superior performance is mainly due to the more efficient optical properties of the starting LB designs. The experimentally observed values in the cases of R_{min}, and R_{max}, and IRL/R_{av} are on the higher side by a margin of 0.1–0.3% over theoretical values which are close to zero. This can be due to either inherent manufacturing errors or measurement errors in the characterization of reflection loss of AR coatings, or to a combination of these errors that are inseparable and unavoidable. The unaccounted losses $A = 1 - 2R_{av} - T_{av}$ are negligible and within the limit of measurement errors as observed in the case of WB AR coatings.

The WB and LB AR coatings are subjected to accelerated environmental tests, and the optical properties are verified before and after each test. The coatings are found to withstand the following tests without any degradation in the optical properties: (1) adhesion as per MIL-M-13508C; (2) abrasion as per MIL-C-675C; (3) humidity as per MIL-C-675C; (4) thermal shock cycling, 70 to −40 °C, 1000 cycles, 5 min dwell time; (5) thermovac cycling 70 to −40 °C, 12 cycles, 2 h dwell time; and (6) hot and cold soak, 70 to −40 °C, 24 h dwell time at each temperature.

From the measured optical properties of WB and LB AR coatings produced from 200 batches, the standard deviation in average transmission T_{av} and average reflection loss R_{av}/R^* is evaluated at the end of every 20 batches of coating production, the results are shown in Fig. 12. The results evidently show that the standard deviation in T_{av} is <0.27%, whereas it is <0.1% in R_{av}. Also, among the 200 batches, there has been no failure in any of the mechanical and environmental tests. These results point out that the manufacturing efficiency of the coatings is better than 99%, which can be attributed primarily to materials selection (particularly Sub2) and strict control of the process parameters. Sub2 coating material has become pivotal in the achievement of coatings of consistent durability that are free of cosmetic defects such as coating spatter and pits.[21]

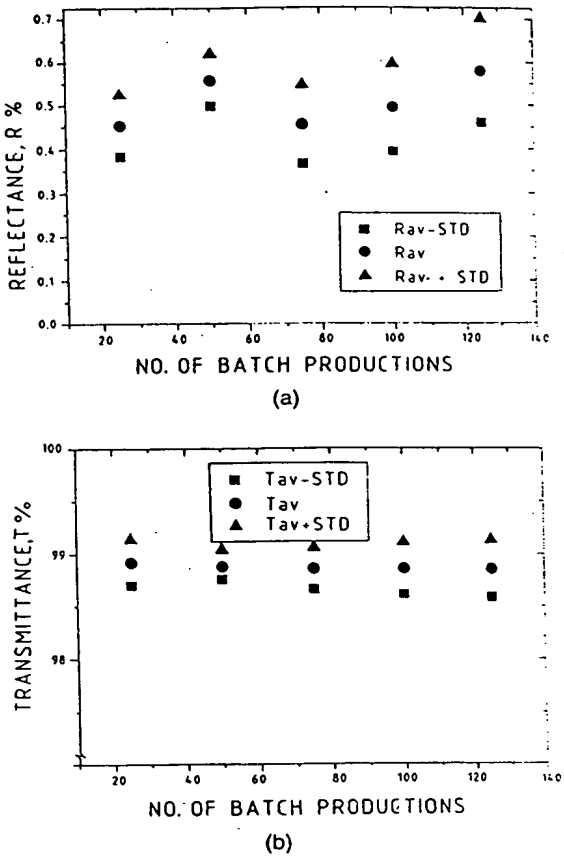

Fig. 12. (a) Standard deviation in reflectance of AR coatings produced in consecutive intervals of batch production. (b) Standard deviation in transmittance of AR coatings produced in consecutive intervals of batch production.

7. Conclusions

The present investigation addressed some of the problems related to visible and near-infrared AR coating design and development. The general conclusions that emerge from the present investigation are

(1) For a given design, IRL R^*, average residual reflection loss R_{av}, and ripple R_{max} are interlinked to the spectral bandwidth of the AR coatings, the higher the bandwidth, the higher the R^*/R_{av} and the R_{max}.

(2) Higher-ripple designs can also have global optical properties (R^*/R_{av} and T_{av}) that are comparable with those of lower-ripple designs but they have higher spectral instability.

(3) Sub2 high-index material in combination with MgF_2 allows the production of efficient AR coatings with the electron-beam evaporation technique, in terms of both optical properties and durability of the coatings.

(4) Soft optical glasses are sensitive to deposition conditions, particularly substrate temperature. By virtue of its having a wider process window Sub2 optical material allows the production of efficient AR coatings on these types of glasses also.

The authors thank the director of the Laboratory for Electro-Optics, Bangalore, and the director of the Indian Space Research Organization Satellite Cen-

tre, Bangalore, for their encouragement and support during this work.

References

1. P. Davi, "High stability coatings for space optics: application to Silex program," in *Space Optics 1994: Space Instrumentation and Spacecraft Optics*, T. M. Dewandre, J. J. Schulte-in-den-Baumen, and E. Sein, eds., Proc. SPIE **2210**, 498–505 (1994).
2. G. K. M. Thutupalli and C. L. Nagendra, "Optical coatings for space applications," Indian J. Phys. A **63**, 661–756 (1989).
3. A. Thelen and R. Langfeld, "Coating design contest: antireflection coatings for lenses to be used with normal and infrared photographic film," in *Thin Films for Optical Systems*, K. H. Guenther, ed., Proc. SPIE **1782**, 552–601 (1992).
4. J. A. Dobrowolski and F. Ho, "High performance step-down AR coatings for high refractive-index IR materials," Appl. Opt. **21**, 288–292 (1982).
5. C. L. Nagendra and G. K. M. Thutupalli, "Design of three-layer antireflection coatings: a generalized approach," Appl. Opt. **27**, 2320–2333 (1988).
6. A. Premoli and M. L. Rastello, "Minimax refining of wideband antireflection coatings for wide angular incidence," Appl. Opt. **33**, 2018–2024 (1994).
7. W. H. Southwell, "Graded index antireflection coatings," Opt. Lett. **8**, 584–587 (1983).
8. H. A. Macleod and E. Pelletier, "Error compensation mechanisms in some thin film monitoring systems," Opt. Acta **24**, 907–930 (1977).
9. C. Grèzes-Besset, F. Chazallet, G. Albrand, and E. Pelletier, "Synthesis and research of the optimum conditions for the optical monitoring of non-quarter-wave multilayers," Appl. Opt. **32**, 5612–5618 (1993).
10. P. J. Martin and R. P. Netterfield, "Optical thin films produced by ion-based techniques," in *Progress in Optics*, E. Wolf, ed. (Permamon, New York, 1989), Vol. 23, pp. 115–182.
11. W. C. Herrmann Jr., "E-beam deposition and characterization of reactively evaporated Ta_2O_5 for optical interference coatings," J. Vac. Sci. Technol. **18**, 1303–1305 (1981).
12. H. G. Shanbhogue, S. Ajith Kumar, M. N. Annapurna, S. N. Prasad, C. L. Nagendra, and G. K. M. Thutupalli, "Visible and near IR antireflection coatings for advanced electro-optical systems," J. Spacecr. Technol. **5**, 16–25 (1995).
13. F. Lepretre, "Lens assemblies for multi spectral camera," in *Space Optics 1994: Space Instrumentation and Spacecraft Optics*, T. M. Dewandre, J. J. Schulte-in-den-Baumen, and E. Sein, eds., Proc. SPIE **2210**, 587–600 (1994).
14. H. K. Pulker, *Coatings on Glass* (Elsevier, Amsterdam, 1984), pp. 20 and 371.
15. R. R. Willey, "Predicting achievable design performance of broadband antireflection coatings," Appl. Opt. **32**, 5447–5451 (1993).
16. A. J. Waldrof, J. A. Dobrowolski, B. T. Sullivan, and L. M. Plante, "Optical coatings deposited by reactive ion plating," Appl. Opt. **32**, 5583–5593 (1993).
17. J. A. Dobrowolski, A. V. Tikhonravov, M. K. Trubetskov, B. T. Sullivan, and P. G. Verly, "Optimal single-band normal-incidence antireflection coatings," Appl. Opt. **35**, 644–658 (1996).
18. K. H. Guenther, "Physical and chemical aspects in the application of thin films on optical elements," Appl. Opt. **23**, 3612–3632 (1984).
19. K. H. Guenther, "Microstructure of vapor-deposited optical coatings," Appl. Opt. **23**, 3806–3816 (1984).
20. M. Cesro and G. Carter, "Ion-beam and dual ion-beam sputter deposition of tantalum oxide films," Opt. Eng. **34**, 596–606 (1995).
21. F. Setter, R. Esselborn, N. Harder, M. Frizona, and P. Folles, "New materials for optical thin films," Appl. Opt. **15**, 2315–2317 (1976).
22. M. Cevro, "Ion-beam sputtering of $(Ta_2O_5)_{1-x}$–$(SiO_2)_{1-x}$ composite thin films," Thin Solid Films **258**, 91–103 (1995).
23. H. W. Zhang and S. X. Liu, "Optical composite film deposited by a double e-gun," Thin Solid Films **209**, 148–149 (1992).
24. J.-S. Chen, S. Chao, J.-S. Kao, H. Niu, and C.-H. Chen, "Mixed films of TiO_2–SiO_2 deposited by double electron beam coevaporation," Appl. Opt. **35**, 90–96 (1996).
25. R.-Y. Tsai, M.-Y. Hua, and F. C. Ho, "Influences of the deposition rate on the microstructure and hardness of composite films prepared by reactive ion-assisted coevaporation," Opt. Eng. **34**, 3075–3082 (1995).
26. C. L. Nagendra and G. K. M. Thutupalli, "Optical constants of infrared (IR) materials in the IR region," J. Spacecr. Technol. **2**, 7–17 (1992).
27. C. L. Nagendra and G. K. M. Thutupalli, "Optical constants of absorbing thin films," Vacuum **31**, 141–145 (1981).
28. R. E. Denton, R. D. Campbell, and S. G. Tomlin, "The determination of optical constants of thin film coating materials," J. Phys. D **5**, 852–863 (1972).
29. J. P. Borgogno, B. Lazarides, and E. Pelletier, "Automatic determination of the optical constants of inhomogeneous thin films," Appl. Opt. **21**, 4020–4029 (1982).
30. H. K. Pulker, "Characterization of optical thin films," Appl. Opt. **18**, 1969–1977 (1979).
31. E. Ritter, "Dielectric film materials for optical applications," in *Physics of Thin Films* G. Hass, M. H. Francombe, and R. K. Hoffman, eds. (Academic, New York, 1975), Vol. 8, pp. 1–49.
32. E. D. Pallick, ed., *Handbook of Optical Constants of Solids*, (Academic, New York, 1991), Vol. II, p. 899.
33. A. S. Valeev, "Determination of the optical constants of weakly absorbing thin films," Opt. Spectrosc. **15**, 269–274 (1963).
34. O. Pierre, I. Asseman, and J. Dauphin, "GOMOS: global ozone monitoring by occulation of stars," in *Space Optics 1994: Earth Observation and Astronomy*, G. Cerutti-Maori and P. Roussel, eds., Proc. SPIE **2209**, 68–77 (1994).
35. A. J. Ratkowski, R. J. Huppi, and M. P. Fetrow, "NIR/SWIR imaging spectrometer for light satellites," in *Space Optics 1994: Earth Observation and Astronomy*, G. Cerutti-Maori and P. Roussel, eds., Proc. SPIE **2209**, 225–235 (1994).
36. M. N. Annapurna, C. L. Nagendra, and G. K. M. Thutupalli, "Software package OPTOSOFT for design of optical coatings," Technical Rep. No. ISRO-ISAC-70-88, 1988 (Indian Space Research Organization, Bangalore, India).
37. M. N. Annapurna, C. L. Nagendra, and G. K. M. Thutupalli, "A new approach to the definition of merit function in numerical optimization methods," presented at the Seventh International Symposium on Thin Films, The Indian Institute of Technology Delhi, The Indian Vacuum Society, New Delhi, India, 7–11 December 1987.
38. M. Born and E. Wolf, *Progress in Optics* (Pergamon, New York, 1970), p. 70.
39. O. S. Heavens and H. M. Liddell, "Least-squares method for automatic design of multilayers," Opt. Acta **15**, 129–138 (1968).
40. M. J. D. Powell, "An efficient method for finding the minimum of a merit function of several variables without calculation of derivatives," Comput. J. **7**, 155–159 (1964).
41. J. Mouchart, "Thin film optical coatings. 1. Optical coating stabilities," Appl. Opt. **16**, 2486–2490 (1977).
42. *Optical Glass*: Supplements and Amendments to Optical Glass Catalogue No. 3111e IX/80, Situation VIII (Schott Glass Technologies, Inc., Germany, 1984).